growth method, and as we have seen, is characteristic of short-circuit-enhanced rather than pure lattice diffusion. In fact, the tracer coefficients found in our work with ZrC and elsewhere for SiC,[25] indicate that the D_0's used by Tobin *et al.*[24] are too low by a factor of 10^2–10^3 and correspondingly, the activation energies are too low by a factor of 1.5 to 2. Furthermore, apart from the seemingly anomolous results of the creep and carburization experiments already mentioned, the rather high (>110 kcal) activation enrgies observed for the tracer work with ZrC and SiC indicates that the mechanism for diffusion may be more complex than that envisioned by Tobin *et al.*[24] At any rate, a mechanism based on the cooperative motion of both species should not be completely rejected at this time.

[25] R. N. Ghoshtagore and R. L. Coble, Phys. Rev. **143**, 623 (1966).

V. CONCLUSIONS

The lattice diffusion coefficient of carbon in zirconium carbide is $1.62\times10^2 \exp(-113\,200/RT)$ cm²/sec. The kinetics of carbide layer growth is controlled by carbon diffusion and the enhancement of material transport along grain boundaries is appreciable. High-temperature creep in zirconium carbide may be controlled by the motion of point defects, but the mechanism is probably not of the Nabarro–Herring type. These conclusions must be altered if the diffusion process involves the cooperative motion of both species.

ACKNOWLEDGMENTS

The authors would like to express their gratitude to Dr. R. W. Kebler who supplied the specimens which made this study possible, and to Professor R. Smoluchowski and Dr. W. S. Williams for their helpful discussions of the results.

JOURNAL OF APPLIED PHYSICS VOLUME 38, NUMBER 4 15 MARCH 1967

Optical Lever Observation of Hypervelocity Impact Shock Waves

VICTOR G. GREGSON, JR.

IIT Research Institute, Chicago, Illinois

(Received 18 August 1966; in final form 11 November 1966)

An optical lever system was used to observe the impact shock wave arrival and free-surface motion at the rear surface of a 2.54-cm-thick 2024-T4 aluminum target plate. The projectile was a 0.636-cm-diam. steel ball and struck the target at a velocity of 5.28±0.11 mm/μsec. The shock-wave data, in the range 30–1 kbar, extend data by Fowles to lower pressures. The measured elastic shock velocity of 6.23±3% agrees with ultrasonic values and with elastic shock values by other investigators.

Elastic shock amplitudes do not maintain a constant value as in one-dimensional experiments, but decay at a rate faster than predicted for spherical elastic waves.

I. INTRODUCTION

THE adaptation of the optical lever technique to hypervelocity impact experiments creates a new tool for investigations in this area. Optical lever observations from one experiment demonstrate agreement with data obtained by explosive experiments and extends shock-wave data to lower values in 2024-T4 aluminum.

The optical lever technique was first used by Allen[1] and by Allen and McCrary[2] to observe spherical shock waves in steel. They used an explosive to generate spherical shock waves, and a streak camera with flash lamp to record shock wave arrivals. Since that time, the technique has been used to observe explosively-produced shock waves in experiments having a plane or two-dimensional steady-state geometry.[3–5] The optical lever technique adapted to record shock waves produced by hypervelocity impact is generally similar to the technique by Allen and McCrary. However, improved experimentation and improved data interpretation permits a more accurate and detailed analysis of experiments than was available to Allen and McCrary.

[1] W. A. Allen, J. Appl. Phys. **24**, 1180 (1953).
[2] W. A. Allen and C. L. McCrary, Rev. Sci. Instr. **24**, 165 (1953).
[3] G. R. Fowles, J. Appl. Phys. **32**, 1475 (1961).
[4] G. E. Duvall and G. R. Fowles, in *High-Pressure Physics and Chemistry*, R. S. Bradley, Ed. (Academic Press Inc., New York, 1963), Vol. 2, Chap. 9.
[5] T. J. Ahrens and V. G. Gregson, Jr., J. Geophys. Res. **69**, 4839 (1964).

II. EXPERIMENT

Figure 1 illustrates a top view of the experiment, showing the equipment and its placement. Light from a flash lamp is turned into the polished target and out again to a streak camera by two 45-deg mirrors. This arrangement insures major pieces of equipment from damage by target perforation.

A continuous-writing streak camera built by Avco is used. The continuous-writing camera is necessary because there may be several milliseconds variation in projectile firing time, as well as a long projectile flight. After the projectile is fired, it passes several viewing ports used to measure projectile velocity.

A UV detector at one port with an appropriate delay time triggers the flash lamp. The flash lamp is

timed such that shock arrival at the polished surface occurs during the period of peak light intensity. The xenon flash lamp is double-pulsed, a technique described by Emmett and Schawlow[6] and by Goncz and Park.[7]

A. Optical Lever Technique

Figure 2 illustrates the optical lever technique. The polished target is placed at the end of a hypervelocity range and the light source grid is placed a fixed distance, d, from the target. An objective lens is used to focus the grid onto the slit plane. A second lens, internal to the camera, focuses the slit onto the film. Lines of light passed by the grid are cut into dots of light by the slit. These dots of light are streaked across the film.

As the projectile strikes the target, the shock wave radiates to the polished surface and is reflected. Because the shock strikes the polished surface at an angle, the surface is turned. This turning angle depends upon the shock strength as well as the emergence angle, and results in an optical lever deflection on the film. Multistepped shock waves produce successive deflections as each step arrives at the polished surface. From the film record, shock velocity and particle velocity can be measured for each step. These values are used with the Rankine-Hugoniot jump conditions[2,5] to compute shock strength, density, and energy.

Shock velocity is calculated as

$$U = U_{\text{app}} \sin c. \tag{1}$$

The apparent velocity U_{app} is measured as the local cotangent of b (in Fig. 2). The emergence angle c is measured by knowing the individual line position on the polished surface relative to impact and by assuming a direct ray path between impact and arrival at the line position.

Particle velocity is calculated as

$$u = [U_{\text{app}} \sin(a/4d)]/\{\cos[c-(a/4d)]\}, \tag{2}$$

where a is the deflection corrected for film demagnification. The usual free-surface approximation is used in computing the particle velocity for the main shock and ramp and is included in the above relation. The relation for particle velocity was described by Ahrens and Gregson and is a general relation for any shock emergence angle; whereas a relation by Fowles is restricted to shallow emergence angles.

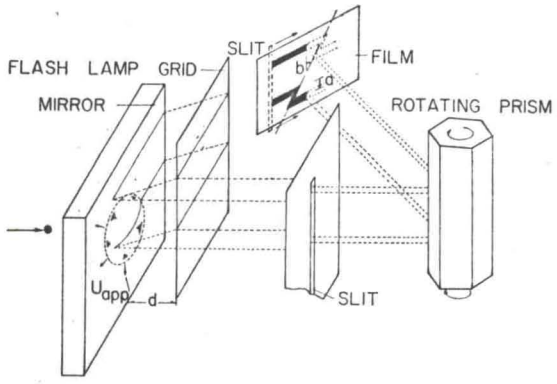

FIG. 2. Optical lever technique.

The free-surface approximation is generally used to compute the amplitude of the elastic shock. This assumes a fluid behavior of the material. The term "pressure" is usually redefined as a "stress" which is normal to the wavefront. Errors in using this assumption for the elastic wave may be as much as 10% of the true stress amplitude. The free-surface approximation has not been used to compute particle velocity and stress of the elastic shock for this experiment. Instead an analysis is used which considers an incident elastic shock reflecting at a free boundary as another dilatational shock and a shear stress shock.

The energy of the incident compressional shock is proportioned between the two reflected shocks as a function of the incidence angle. From energy considerations of any shock, the total energy is partitioned equally between internal and kinetic energy. For most elastic shocks, the stresses are such that the slight temperature increase behind the shock front results in little of the available internal energy lost to propagate the shock. Assuming no energy is lost, the kinetic energy of an incident elastic shock can be proportioned between the kinetic energy of the two reflected shocks. The kinetic energy of a unit volume for the incident shock is

$$E = 1/2\rho_0 u_1^2, \tag{3}$$

where E is the kinetic energy, u_1 is the particle velocity, and ρ_0 is the material density before the shock arrival. The kinetic energy of a unit volume of the reflected shocks is

$$E = 1/2\rho_0 (u_2+u_3)^2, \tag{4}$$

where u_2 and u_3 are particle velocities of the dilational and shear-stress shocks respectively. If it is assumed that errors in an infinitesmal-amplitude-elastic-wave analysis are small compared to a finite-amplitude-wave analysis, the reflected shock particle velocities can be described in terms of the incident particle

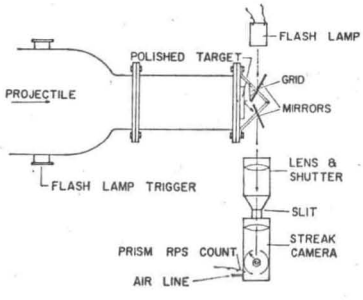

FIG. 1. Top view of optical lever experiment.

[6] J. L. Emmett and A. L. Schawlow, Appl. Phys. Letters **2**, 204 (1963).

[7] J. H. Goncz and S. W. Park, Microwaves, p. 34 (1965).

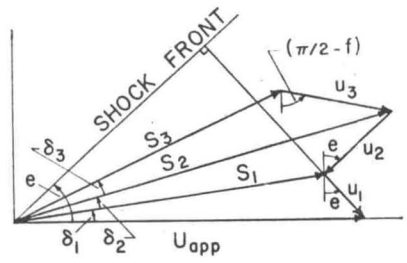

FIG. 3. Two-dimensional flow diagram for incident and reflected elastic shocks. Shock incidence and reflection results in streamlines S_1, S_2, and S_3 giving a surface rotation $\delta_1+\delta_2+\delta_3$.

velocity[8] as

$$u_2^2=(A_2/A_1)^2u_1^2, \tag{5}$$

and

$$u_3^2=(B_2/A_1)^2(\phi/\Psi)u_1^2. \tag{6}$$

A_2/A_1 is the amplitude ratio of the reflected compressional wave to the incident compressional wave. B_2/A_1 is the amplitude ratio of the reflected shear wave to the incident compressional wave. C_p and C_s are velocities for the compressional and shear waves respectively in

$$\phi[(U_{\rm app}^2/C_p^2)-1]^{1/2}=\tan(\pi/2-e), \tag{7}$$

and

$$\Psi=[(U_{\rm app}^2/C_s^2)-1]^{1/2}=\tan(\pi/2-f). \tag{8}$$

The angle e is the angle between the free-surface and the incident compressional wave. The angle f is the angle between the free-surface and the reflected shear wave. The amplitude ratios are

$$\frac{A_2}{A_1}=\frac{4\mu\phi\Psi-(\Psi^2-1)[\lambda+\phi^2(\lambda+2\mu)]}{4\mu\phi\Psi+(\Psi^2-1)[\lambda+\phi^2(\lambda+2\mu)]} \tag{9}$$

and

$$\frac{B_2}{A_1}=\frac{-4\mu\phi[\lambda+\phi^2(\lambda+2\mu)]}{4\mu^2\phi\Psi+(\Psi^2-1)[\lambda+\phi^2(\lambda+2\mu)]}, \tag{10}$$

where λ and μ are Lame′ constants.

The optical lever deflection can be related to the particle velocity $\mathbf{u}_1$ by extending the flow diagram of a hydrodynamic shock described in Ahrens and Gregson. This extension (see Fig. 3) will not depend upon the usual approximation that the free-surface velocity is twice the particle velocity. Instead, the optical lever deflection is equated to the surface rotations produced by each of the three shocks

$$1/2ad^{-1}=\delta_1+\delta_2+\delta_3, \tag{11}$$

where δ_1, δ_2, and δ_3 are the rotations associated with the incident compressional shock, the reflected dilatational shock, and the reflected shear stress shock respectively.

[8] W. M. Ewing, W. S. Jardetzky, and F. Press, *Elastic Waves in Layered Media* (McGraw-Hill Book Company, Inc., New York, 1957), Chap. 2, Sec. 2-1.

From the geometry of Fig. 3,

$$\delta_1=\tan^{-1}[u_1\cos e/(U_{\rm app}-u_1\sin e)]. \tag{12}$$

The surface rotation of the reflected compressional rarefaction is

$$\delta_2=\tan^{-1}\{u_2\cos(e+\delta_1)/[S_1-u_2\sin(e+\delta_1)]\}, \tag{13}$$

where the streamline $\mathbf{S}_1$ has a magnitude

$$S_1=[(U_{\rm app}-u_1\sin e)/\cos\delta_1]. \tag{14}$$

The surface rotation of the reflected shear stress rarefaction is

$$\delta_3=\tan^{-1}\left[\frac{u_3\cos(\pi/2-f-\delta_1-\delta_2)}{S_2-u_3\sin(\pi/2-f-\delta_1-\delta_2)}\right], \tag{15}$$

where the streamline $\mathbf{S}_2$ has a magnitude

$$S_2=\{[S_1+u_2\sin(e+\delta_1)]/\cos\delta_2\}. \tag{16}$$

Equations (5) to (16) are used in a digital computer program to find values of u_1, the incident compressional shock particle velocity. The necessary elastic wave velocities, material constants, and apparent velocity are used to calculate the amplitude ratios relating particle velocities u_2 and u_3 to u_1. Values of u_1 are selected and used in Eqs. (12) to (16) until Eq. (11) is valid to the numerical precision required in the experiment. Such values are 5% to 10% less than particle velocities computed by the free-surface approximation.

An additional feature to consider in this experiment that does not concern a plane wave or a two-dimensional steady-state experiment is an impact off the optic axis of the optical lever alignment. Figure 4 illustrates the geometry of this case. Assume an off-axis impact

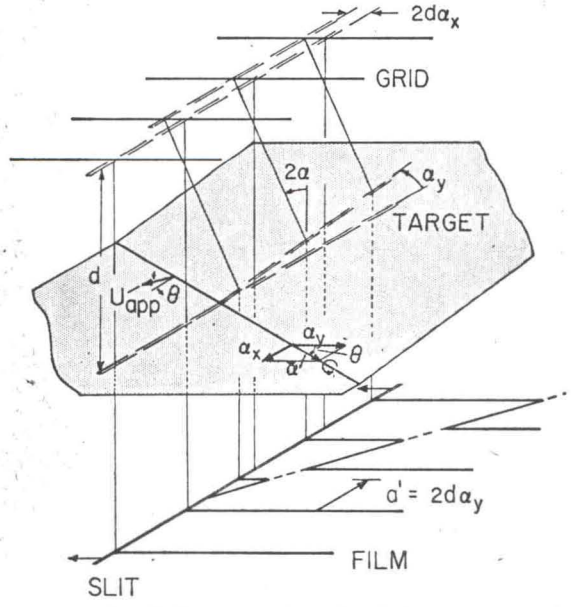

FIG. 4. Geometry of an off-axis impact.

TABLE I. Summary of experimental data.

Distance from impact (mm)	Elastic shock		Ramp	Main shock	
	Shock velocity (mm/μsec)	Particle velocity (mm/μsec)	Particle velocity (mm/μsec)	Shock velocity (mm/μsec)	Particle velocity (mm/μsec)
43.9	6.18	0.010	...	...	...
42.0	6.17	0.013	...	(5.6)	0.030
40.1	6.14	0.013	...	(5.6)	0.031
38.2	6.24	0.016	0.028	5.61	0.038
35.6	6.22	0.017	0.038	5.57	0.059
33.1	6.27	0.017	0.037	5.54	0.062
31.6	6.06	0.017	0.038	5.55	0.076
30.3	6.14	0.017	0.037	5.47	0.087
29.0	6.23	0.018	0.039	5.47	0.099
27.9	6.36	0.020	0.040	5.71	0.108
27.0	6.34	0.023	0.052	6.29	0.131
26.2	...	0.032	...	(6.70)	0.154
25.6	6.18	0.035	...	(6.72)	0.161
26.2	6.44	0.027	0.058	6.07	0.143
27.0	6.36	0.023	0.047	6.07	0.130
27.9	6.18	0.023	0.047	5.78	0.113
29.0	6.23	0.021	0.051	5.58	0.112
30.3	6.16	0.020	...	5.34	0.100

Average 6.23±3%

and a shock wave breakout that occurs at a local attitude angle θ with the slit projection at the target.

The optical details are omitted for clarity. One objective lens focuses the slit plane onto the film, hence the slit and film planes are shown as coincident. The polished surface is within the field depth of the other objective lens focusing the grid onto the slit plane, hence the camera slit and grid are shown on opposite sides of the polished target with sets of ray paths as parallel lines. The surface is turned at the breakout and is represented by a rotation vector $\boldsymbol{\alpha}$, parallel to the breakout line, and a unit vector $\mathbf{k}$, perpendicular to the target surface. The shock breakout line moves across the target with an apparent shock velocity U_{app}.

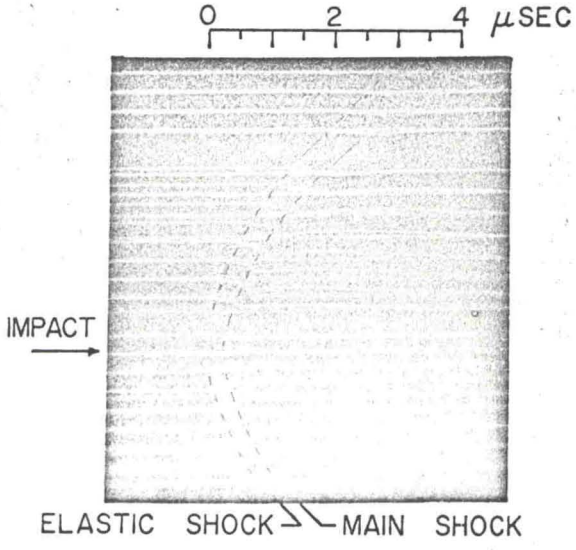

FIG. 5. Photograph of an optical lever record. The two-step shock front shows the elastic shock wave followed by the main shock wave. Lines which show no deflection are camera rewrite indicating a permanent deformation of the target.

Let x, y, z be a rectangular coordinate axis such that x lies along the slit, and z is directed along the optic axis. Each deflected ray is rotated $2\boldsymbol{\alpha}$. The displacement of a ray at the grid plane is

$$2\boldsymbol{\alpha}\times\mathbf{r}=\begin{vmatrix}\mathbf{i} & \mathbf{j} & \mathbf{k}\\ 2\alpha_x & 2\alpha_y & 0\\ 0 & 0 & d\end{vmatrix}=2d\alpha_y\mathbf{i}-2d\alpha_x\mathbf{j}. \quad (17)$$

It is apparent that this relation is similar to the relation

$$\alpha=a/2d \quad (18)$$

described by Fowles, Duvall and Fowles, and by Ahrens and Gregson. Thus the deflection related to turning angle is

$$\alpha=a/2d\cos\theta, \quad (19)$$

and can be used to correct Eqs. (2) and (11) through the appropriate free surface relations for the effect of an off-axis impact. The shock breakout rate along the slit is $U_{\text{app}}\cos\theta$.

B. Results

Figure 5 is an optical lever record obtained by hypervelocity impact of a 2.54-cm-thick target of 2020-T4 aluminum. The projectile was a steel ball 0.636 cm in diameter and struck the target at a velocity of 5.28±0.11 mm/μsec. The elastic shock wave followed by the decaying main shock wave is clearly evident. Table I lists values of measured shock and particle velocity.

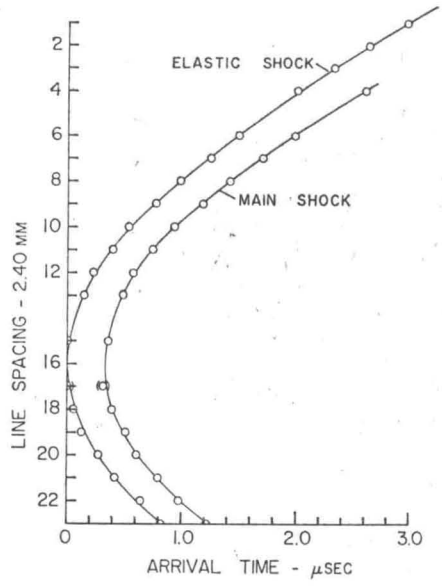

FIG. 6. Plot of shock-wave arrival across the target free-surface.

Figure 6 is a time–distance plot of the shock breakout at the polished target interface. The value of line spacing is accurate to ± 0.01 mm and shock arrival times are accurate to ± 0.04 μsec. Figure 7 compares data obtained by Fowles with data obtained in this experiment. For values of the elastic shock, the term "pressure" is interpreted as stress normal to the shock front. For data by Fowles, pressure values are accurate to $\pm 3\%$ and particle velocity values are accurate to $\pm 5\%$. Pressure values for the hypervelocity impact experiment are accurate to $\pm 5.5\%$ and particle velocity values are accurate to $\pm 8\%$. Pressure decay through the target is plotted in Fig. 8. Pressure decay of the main shock wave ranges from the inverse cube of the distance at higher pressure values to the inverse square of the distance at lowest pressure values. Maximum pressure values of the ramp between the main shock front and the elastic shock front maintain a constant pressure of 6.0 ± 0.5 kbar except near the initial breakout. The elastic shock wave decays from at least 6.2 ± 0.4 kbar to 1.5 ± 0.2 kbar. The elastic shock decays as the inverse square of the distance over the observed stress range. Small amplitude elastic waves from a spherical source theoretically decay as the inverse of the distance. The peak amplitude of the elastic shock, 6.2 ± 0.4 kbar, agrees with the nondecaying Hugoniot elastic limit measured in simpler geometries. The value of the elastic shock velocity is 6.23 ± 0.19 mm/μsec and agrees with ultrasonic measurements and measurements by Fowles.

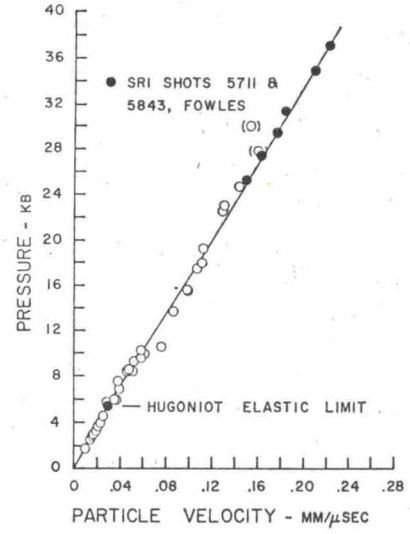

FIG. 7. Plot of pressure as a function of particle velocity, 2024-T4 aluminum.

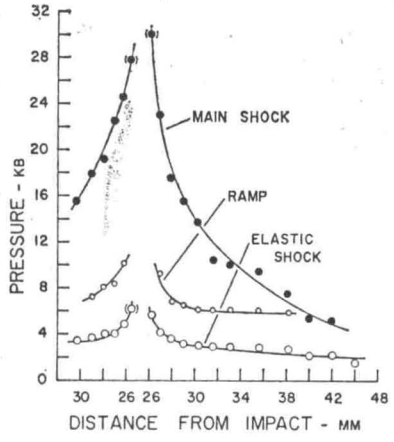

FIG. 8. Shock-wave decay as a function of distance traveled through the target.

III. CONCLUSIONS

The optical lever technique of observing shock waves is extended to hypervelocity impact experiments. A general relation for particle velocity is extended to elastic shocks and to the case of an impact off the optic axis of the experiment. An experiment using the above relation illustrates the technique. Consistent results are obtained between data from this experiment and data by Fowles. Data also extend into the pressure region below 30 kbar for 2024-T4 aluminum. The decay rate of the elastic shock wave is faster than the theoretical prediction that the amplitude should decrease as the inverse of the distance.

ACKNOWLEDGMENTS

The author wishes to thank T. A. Zaker for many helpful discussions. T. A. Zaker also contributed to the correction for an off-axis impact. The author also wishes to thank F. J. Zimmerman and H. H. Nagaoka for use of and help with the hypervelocity gun facilities. They also providedadditional information such as projectile velocity.